



Contents lists available at ScienceDirect

Journal of Power Sources

journal homepage: www.elsevier.com/locate/jpowsour

Facile preparation of polypyrrole/graphene oxide nanocomposites with large areal capacitance using electrochemical codeposition for supercapacitors



Haihan Zhou*, Gaoyi Han*, Yaoming Xiao, Yunzhen Chang, Hua-Jin Zhai

Institute of Molecular Science, Key Laboratory of Chemical Biology and Molecular Engineering of Education Ministry, Shanxi University, Taiyuan 030006, China

HIGHLIGHTS

- PPy/GO nanocomposites were fabricated by facile electrochemical codeposition.
- The areal capacitance of conducting polymer/GO composites is firstly reported.
- The composites reveal large areal capacitance and superior cycle stability.
- The deposition time affects the capacitive behavior of the composites obviously.

ARTICLE INFO

Article history:

Received 7 February 2014
Received in revised form
10 April 2014
Accepted 10 April 2014
Available online 18 April 2014

Keywords:

Supercapacitor
Areal capacitance
Conducting polymers
Graphene
Nanocomposites

ABSTRACT

A simple and low-cost electrochemical codeposition method has been introduced to fabricate polypyrrole/graphene oxide (PPy/GO) nanocomposites and the areal capacitance of conducting polymer/GO composites is reported for the first time. Fourier transform infrared spectroscopy (FTIR), Transmission electron microscopy (TEM), X-ray photoelectron spectroscopy (XPS), and X-ray diffraction (XRD) are implemented to determine the PPy/GO nanocomposites are successfully prepared and the interaction between PPy and GO. The as-prepared PPy/GO nanocomposites show the curly sheet-like morphology, superior capacitive behaviors and cyclic stability. Furthermore, the varying deposition time is implemented to investigate the impact of the loading amount on electrochemical behavior of the composites, and a high areal capacitance of 152 mF cm^{-2} is achieved at 10 mV s^{-1} CV scan. However, the thicker films caused by the long deposition time would result in larger diffusion resistance of electrolyte ions, consequently exhibit the relatively lower capacitance value at the high current density. The GCD tests indicate moderate deposition time is more suitable for the fast charge/discharge. Considering the very simple and effective synthetic process, the PPy/GO nanocomposites with relatively high areal capacitance are competitive candidate for supercapacitor application, and its capacitive performances can be easily tuned by varying the deposition time.

© 2014 Elsevier B.V. All rights reserved.

1. Introduction

As a type of electrochemical energy storage device, supercapacitors have attracted considerable attention over the past decades. Owing to the higher power density and longer cycle life than secondary batteries and higher energy density compared to conventional capacitors, they are applicable in some systems such as hybrid electric vehicles, portable electronics, mobile

communications, etc., and are believed to have potential to fill the power/energy gap between traditional dielectric capacitors and batteries/fuel cells [1–5].

Currently, a major limitation of state-of-art supercapacitors lies in their relatively low energy density compared with batteries/fuel cells [6]. It is well known that the electrode material is a key component that determines supercapacitor's capacity, so a large number of researches have been made to develop new high-performance electrode materials [7–10]. Generally, the charge storage mechanism of supercapacitors could be classified into two types: electrochemical double layer capacitors (EDLCs) and faradaic pseudocapacitors (also referred to as redox supercapacitors). The

* Corresponding authors. Tel.: +86 351 7010699; fax: +86 351 7016358.

E-mail addresses: hhzhou@sxu.edu.cn (H. Zhou), han_gaoyis@sxu.edu.cn (G. Han).

former capacitance comes from the pure electrostatic charge accumulated at the electrode/electrolyte interface, and the electrodes were mainly based on carbon materials including activated carbon, carbon nanotubes, and graphene etc., while the latter energy is stored by a fast and reversible faradaic redox reaction on the electrode surface formed with electroactive materials, such as transition metal oxides and conducting polymers [11–13]. Researches show that each electrode materials has its advantage and disadvantage. Commonly, carbon materials show high power density and long cycle life but low capacitance [14]. While transition metal oxides have higher energy density than carbon materials and better cycling stability than conducting polymer materials, but exhibit a drawback of poor conductivity [15]. Conducting polymers possess high energy density, but they exhibit the disadvantage of a low cycle life because swelling and shrinkage may occur during doping/dedoping processes [16]. Based on the mentioned characteristic of different electrode materials above, considerable attention has been devoted to exploring hybrid of different materials to obtain high-performance capacitive electrode materials. Yang et al. [17] reported cobalt monoxide (CoO)-doped graphitic porous carbon microspheres effectively combined the electric double-layer capacitance and pseudo-capacitance when used as the electrode in supercapacitor, which led to a higher operation voltage and gave rise to a significantly higher energy density. Wei et al. [18] prepared polyaniline (PANI)/graphite oxide nanocomposite films by electropolymerization of aniline monomers onto graphite oxide-coated conducting glass slides with spin coating technique, which demonstrated a much more enhanced durability than the pure PANI films. So this study would be devoted to developing the composite electrode materials combining advantages of double-layer capacitance and pseudocapacitance, which contribute indivisible to the total electrochemical capacitance value of a supercapacitor.

PPy is the important material for electrodes of supercapacitors due to its high specific capacitance and electrical conductivity, low cost and chemical stability, however, it exhibits poor stabilities during the charge/discharge process [19,20]. Graphene, a single atomic plane of graphite, is regarded as an excellent electrode material for supercapacitors due to its high specific surface area, superior electrical conductivity, and chemical stability, but the capacitance values are limited by the microstructures in the materials [21,22]. Therefore, based on the complementary properties of PPy and graphene, considerable efforts have been made to incorporate graphene or its derivatives into PPy-based composite materials. The study by Biswas [23] showed the composite electrode of graphene nanosheets and polypyrrole nanowires has a high specific capacitance of $\sim 165 \text{ F g}^{-1}$ with a nearly ideal rectangular cyclic voltammogram at increasing voltage scan rates and high electrochemical cyclic stability. Mini et al. [24] prepared the high-performance supercapacitor electrodes with electrophoretic deposition of graphene, upon which the PPy layer was electropolymerized. Lim et al. [25,26] reported the electrochemical polymerization of polypyrrole/graphene (PPy/GR) using sodium p-toluenesulfonate (NapTS) as a supporting electrolyte, which indicated the presence of graphene enhanced the electrochemical performances of PPy tremendously. Some efforts have been made on the composites of graphene with conducting polymer, it is still a challenge to synthesize conducting polymer/graphene composites as electrode materials with the high capacitance, good rate performance, and cycle stability for supercapacitors, and what's more, almost all the related researches focus on the mass specific capacitance of electrode materials. Up to date, no work has been reported on the investigation of areal capacitance of conducting polymers/GO nanocomposites. For applications such as small scale electronics and

stationary energy storage devices where areal capacitance is a better indicator of the supercapacitor performance than mass specific capacitance although the mass specific capacitance has always been used in the literature for comparison of the supercapacitor performance [27,28].

In this research, PPy/GO nanocomposites electrodes were fabricated using a facile one-step electrochemical co-electrodeposition method. The influence of deposition time (i.e. deposition amount) on the capacitive performances including areal capacitance of the PPy/GO nanocomposites electrodes was investigated, and the performance of three type of representative nanocomposites electrodes with varying deposition time were compared detailedly. The compositions and morphology as well as the structures of the composite films were studied using Fourier transform infrared spectroscopy (FT-IR), Transmission electron microscopy (TEM), X-ray photoelectron spectroscopy (XPS), X-ray diffraction (XRD), and scan electron microscope (SEM), electrochemical behaviors of composite films were investigated using cyclic voltammetry (CV) and galvanostatic charge/discharge measurements (GCD) and electrochemical impedance spectroscopy (EIS).

2. Experimental

2.1. Reagents and materials

Natural graphite powder (325 mesh) was purchased from Tianjin Guangfu Research Institute. Pyrrole (A.R., Shanghai Chemical Reagent) was purified through distillation under reduced pressure and stored at a temperature less than 5°C . FTO conducting glasses were obtained from Dalian Heptachroma SolarTech (DHS-FTO22-8-02, $8 \Omega \square^{-1}$), $10 \text{ mm} \times 10 \text{ mm}$ conductive areas were exposed as the electrochemical codeposited substrate. Prior to use, the glasses were ultrasonically cleaned in acetone and deionized water successively.

2.2. Electrochemical codeposition of PPy/GO nanocomposites

GO was prepared by oxidizing the natural graphite powder and subsequent exfoliation by ultrasonication according to the method reported in literature [29,30]. The obtained GO aqueous dispersion was treated with freeze drying and preserved at the room temperature. During the procedure of deposition, an aqueous solution containing 0.25 M pyrrole monomer and 2 mg mL^{-1} GO was dispersed under ultrasonication for about 15 min to form a metastable homogenous colloidal solution, which could last for more than 24 h at room temperature. After that, PPy/GO nanocomposites were electrodeposited onto the FTO conducting glasses in a galvanostatic mode (Fig. 1a), which a current of 1.0 mA cm^{-2} was applied for varying time ranging from 200 to 2700 s. After the electrodeposition, the composites-coated glasses were washed with adequate deionized water to remove the unreacted substance, followed by drying at room temperature under ambient air environment, which is exhibited in Fig. 1b. During the deposition, the cleaned FTO conducting glasses were fixed in a two-electrode cell with a large-area Pt sheet acting as the counter electrode and pseudo-reference electrode. For FT-IR test, pure PPy was deposited from solutions containing 0.25 M pyrrole monomer and 1 M KCl with the same procedure.

2.3. Characterization

2.3.1. Components and structures analysis

PPy and PPy/GO films were scraped from the surface of films deposited onto FTO conducting glasses for the FT-IR, TEM, XPS, and

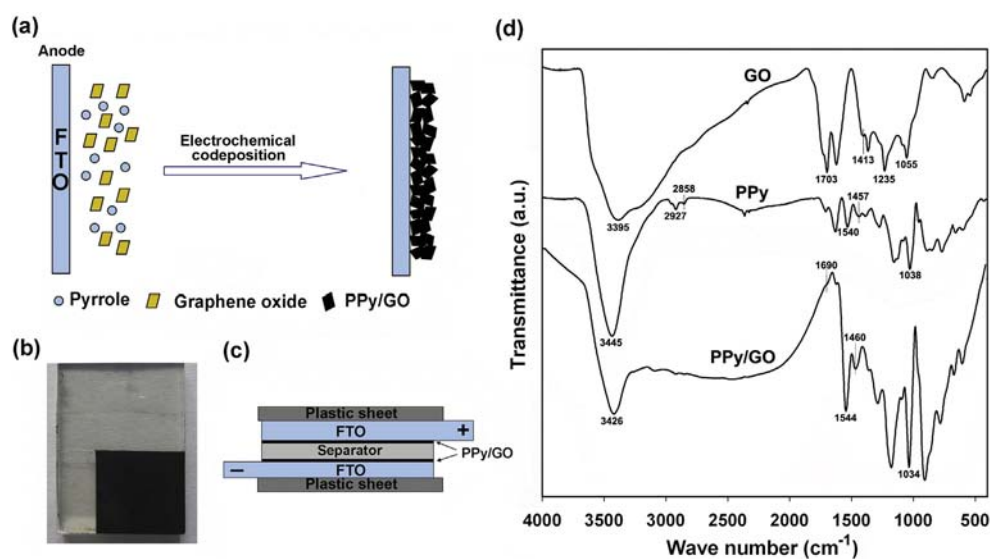


Fig. 1. (a) The schematic diagram for the electrochemical codeposition of PPy/GO nanocomposites; (b) The real photo of PPy/GO-deposited FTO conducting glass; (c) The construction of capacitor cells for electrochemical measurements; (d) FT-IR spectra of GO, PPy, and PPy/GO.

XRD tests. FT-IR spectra were obtained with a Bruker Tensor 27 FT-IR Spectrometer within the range of 4000–400 cm^{-1} , and all samples were prepared by potassium bromide tableting. X-ray photoelectron spectroscopy (XPS) measurements were performed using a Krato Axis Ultra DLD spectrometer with Al $K\alpha$ X-ray ($h\nu = 1486.6$ eV) at 15 kV and 150 W. The X-ray diffraction (XRD) patterns of the samples were recorded on a Bruker D8 Advance X-ray diffraction meter with Cu $K\alpha$ radiation and graphite monochromator, at the scan speed of 5°min^{-1} with a step size of 0.02° .

2.3.2. Morphology characterization

The microstructures of the PPy/GO and GO were examined with a high resolution transmission electron microscopy (TEM, JEM-2100, JEOL) operating at 200 kV. The surface morphology of the PPy/GO-deposited FTO was observed using a field emission scan electron microscope (SEM, JSM-6701F, JEOL) operated with a voltage of 10.0 kV.

2.3.3. Electrochemical measurements

For the electrochemical measurements, the capacitor cells (Fig. 1c) were assembled by using two pieces of PPy/GO-deposited FTO conducting glasses (one oxidized and one reduced) as the two electrodes, a filter paper soaked with 1.0 M KCl was used as the electrolyte to separate the two pieces of conducting glasses, the conducting glasses itself was used as the current collector and two pieces of PVC plate were utilized to coat and stabilize the cell. All the electrochemical measurements were carried out on an electrochemical workstation (CHI 660B, Chenhua, China) using two-electrode system. The CV measurements were performed between potentials of -0.5 V to 0.5 V, and the scan rates ranged from 1 to 800 mV s^{-1} . The GCD tests were performed at varying current density with the cutoff voltage of -0.5 V and 0.5 V. The EIS were measured using 5 mV (rms) AC sinusoid signal and at a frequency range from 100 kHz to 0.01 Hz at the open circuit potential. During the aforementioned electrochemical tests, the assembled cells were wrapped with a preservative film to prevent the volatilization of electrolyte.

In order to analyze the variation of capacitance with varying scan rates, the areal capacitance (C_S) value of the nanocomposites

can be calculated based on CV curves according to following equation (1):

$$C_S = \left(\int idV \right) / (S \times \Delta V \times \nu) \quad (1)$$

where C_S is the areal capacitance in F cm^{-2} , $\int idV$ the integrated area of the CV curve, S the surface area of active materials in the single electrode in cm^2 and it is fixed at 1 cm^2 in this study, ΔV the scanned potential window in V and ν the scan rate in V s^{-1} .

The galvanostatic charge/discharge measurements by chronopotentiometry were also performed to evaluate the areal capacitance of the nanocomposites using the equation (2):

$$C_S = (2 \times i \times t) / (S \times \Delta V) \quad (2)$$

where C_S is the areal capacitance in F cm^{-2} , i the discharge current in A, t the discharge time in s, S the surface area of the active materials on the single electrode in cm^2 and ΔV the scan potential window in V.

The areal energy density and power density of the nanocomposites depicted in the Ragone plot can be calculated by using the Equations (3) and (4), respectively.

$$E = \frac{1}{2} C_S \Delta V^2 \quad (3)$$

$$P = \frac{3600E}{t} \quad (4)$$

where E is the areal energy density in Wh cm^{-2} , P the areal power density in W cm^{-2} , C_S the areal capacitance in F cm^{-2} , ΔV the potential window (excluding iR drop in the beginning of the discharge) in V and t the discharge time in s.

3. Results and discussion

3.1. Components and structures analysis

During the process of electrochemical polymerization, the anionic GO served as a counter-ion was entrapped in the PPy

nanocomposites and also acted as an effective charge balancing dopant within the PPy. FT-IR measurements were made to demonstrate the formation of PPy/GO nanocomposites and the spectra of GO, PPy and PPy/GO nanocomposites are shown in Fig. 1d. In the spectrum of GO, the broad peak at 3395 cm^{-1} and peak at 1703 cm^{-1} can be attributed to O–H stretching vibration and the C=O stretching of carbonyl, respectively. The peaks observed at 1413 cm^{-1} and 1235 cm^{-1} represent the O–H deformation and C–OH stretching vibration, in addition, the peak at 1055 cm^{-1} is the characteristic peak of epoxide group [31]. In the spectra of PPy, the peaks at 1540 , 1457 , and 3445 cm^{-1} are associated with the C–C, C–N, and N–H stretching vibration in the pyrrole ring, respectively. The peaks located at 2927 and 2858 cm^{-1} are designated as the asymmetric stretching and symmetric vibrations of $-\text{CH}_2$ [32,33]. As expected, the characteristic peaks of PPy appear at 1544 and 1460 cm^{-1} in the PPy/GO spectra, suggest the presence of PPy in the PPy/GO composite. It should be noted that the peak due to the C=O of COOH group within the PPy/GO has been downshifted to 1690 cm^{-1} which is probably due to the π – π interactions and hydrogen bonding between the GO layers and aromatic polypyrrole rings. Also it has been observed that the peak at 1038 cm^{-1} which is obtained due to the C–H in-plane vibration of PPy ring, is shifted to 1034 cm^{-1} [34,35]. FT-IR results clearly show that the characteristic peaks of individual components and reveal the presence of PPy and GO in the composite as well as the successful combination of both components.

TEM characterization was used to investigate the composite morphology between PPy and GO, and the TEM images were shown in Fig. 2a. As expected, the GO shows the sheet-like morphology with smooth and slightly curly edge, meanwhile, the nanosheets present a large surface area. Compared to the GO, PPy/GO displays the overlap structure with multilayer GO nanosheets, and the PPy particles are decorated dispersedly on the surface and intercalates between the GO sheets. It is also observed that the PPy/GO composite sheets are folded with some dark area that indicates the flexible character of the nanocomposites. TEM images reveal that the GO and PPy form a nanocomposite with the PPy coated on the two-dimensional GO surface and/or filled between the GO nanosheets.

XPS measurements are used to characterize the elemental composition of as-prepared PPy/GO nanocomposites. The deconvoluted C 1s core level XPS spectra of GO, PPy, and PPy/GO and N 1s XPS spectra of PPy and PPy/GO are shown in Fig. 2b. The C 1s XPS spectrum of GO shows the peak centered at 284.4 eV originates from C=C bonds formed by sp^2 carbon, and the peak at 285.0 eV is ascribed to C–C bonds formed by sp^3 carbon. The fitted peaks located at higher binding energies are attributed to the sp^3 carbon with different C–O bonding configurations, they are the groups of C–O, C=O and O–C=O located at about 286.6 , 287.1 , and 288.5 eV , respectively [11]. In addition, it can be calculated that the proportion of O–C=O in various C species is only 10.6% based on the areas of fitted peaks, indicating the GO possess a small amount of carboxyl group as the counter ions, which results in the relatively less pyrrole polymerized and dispersedly coated on the GO just as shown in the TEM image of PPy/GO (Fig. 2a). For the C 1s XPS spectrum of the PPy, four component peaks centered at 284.2 , 285.1 , 286.0 , and 287.6 eV , which originates from sp^2 carbon, sp^3 carbon, C–N, and C=O, respectively, it should be noted that the C=O peaks in PPy spectrum suggest that some over-oxidation have occurred during the electropolymerization [36]. The C 1s core level XPS of the PPy/GO composites could be fitted into six component peaks located at 284.1 , 285.0 , 285.5 , 286.6 , 287.3 , and 288.9 eV , which are attributed to sp^2 hybridized carbon, sp^3 hybridized carbon, C–N, C–O, C=O, and O–C=O, respectively. The detected C–N in PPy/GO C 1s XPS spectra originates from PPy, and the ratio based on the XPS spectra of various elements for C/O of PPy/GO is bigger than that of GO due to the presence of PPy coated on the GO. Moreover, N element content in the PPy is 21.3 at.%, while it decrease to 10.6 at.% in the PPy/GO, indicating the relatively large amounts of GO exist in the nanocomposites. For N 1s XPS spectrum of PPy, the low binding energy (BE) component at 397.6 eV is assigned to the imine nitrogen ($-\text{N}=\text{}$), the major component at 399.7 eV is assigned to neutral pyrrolylium nitrogen ($\text{N}-\text{H}$), the high-BE component at 400.8 eV is assigned to the positively charged nitrogen atom ($-\text{N}^+$). The presence of $-\text{N}^+$ indicates that the PPy component are doped, i.e., PPy are in the oxidized state. The $-\text{N}^+$ polaron is critical for PPy to exhibit conductive, because the direct electrostatic interaction between the positive charge and

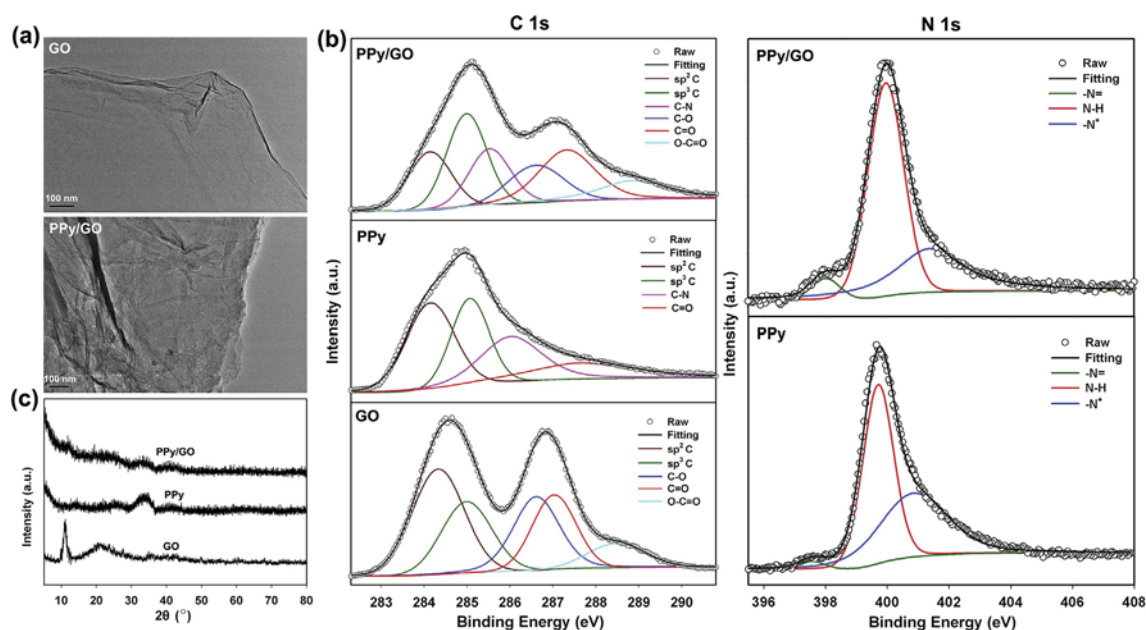


Fig. 2. (a) The representative TEM images of GO and PPy/GO; (b) C 1s XPS spectra of GO, PPy, and PPy/GO and N 1s XPS spectra of PPy and PPy/GO; (c) XRD patterns of GO, PPy, and PPy/GO.

electron facilitates the conduction [37]. Similarly, N 1s XPS spectrum of PPy/GO also shows three component peaks originates from $-N=$, $N-H$, and $-N^+$, but the BE shifted to higher region with peaks appearing at 398.0, 400.0, and 401.4 eV, respectively, it might be due to the $\pi-\pi$ stacking between the PPy and GO layers, which is in accordance with the FT-IR results. In addition, considering the doping reaction mechanism [38], the GO as dopant, serving as electron acceptor, forms a complex with PPy (π electron donor of the pyrrole rings) leading to the structure of $D^{\delta+}$, ..., $A^{\delta-}$, so the complex keeps neutral with the formation of $-N^+$ in the PPy of oxidized state.

The obtained PPy/GO nanocomposites were further confirmed by XRD, as shown in Fig. 2c. XRD pattern of the GO revealed an intense, sharp peak centered at $2\theta = 10.9^\circ$, corresponding to a layer-to-layer distance (d -spacing) of 0.81 nm of the GO sheets according to the Bragg equation. This value is larger than the d -spacing (0.335 nm) of pristine graphite ($2\theta = 26.6^\circ$) due to the introduction of oxygenated functional groups and intercalated water molecules between layers [39,40], while the broad peak at 21.4° indicates that the GO sheets exhibit some aggregations [11]. The PPy, exhibit a weak and broad diffraction peak at $2\theta = 22-35^\circ$, which suggests that the PPy is amorphous in nature [41]. Almost no obvious peaks can be observed from the PPy/GO plot except for the weaker peak situating at 33° , which is related to the diffraction peak of PPy. Moreover, the peak ascribed to GO within these nanocomposites almost disappeared, indicating the coating of scattered PPy particles between the GO nanosheets increase the d -spacing of the layered GO.

3.2. Capacitive properties of PPy/GO nanocomposites

CV and GCD tests were carried out to investigate the capacitive performance of the PPy/GO nanocomposites electrodes. It can be seen from Fig. 3a that the curves at different scan rates do not show obvious redox peaks in the whole potential range, indicating that the electrode was charged and discharged at a pseudo-constant rate over the whole CV process, it is because that capacitor assembled by two pieces of PPy/GO-deposited FTO electrodes were tested by two-electrode system, during the test, one piece of composites electrode was oxidized while the other was reduced, which resulted in the oxidation/reduction peaks of PPy unobvious and showed the rectangular CV shape. The rectangular-like CV curves with the almost symmetric I-E responses can be observed at all scan rates ranging from 10 to 200 mV s^{-1} and the obvious increase of current with scan rates, which indicate that the nanocomposites exhibit ideal capacitive behavior for rapid charge and discharge, so the composites can be used as the candidate for electrochemical capacitors.

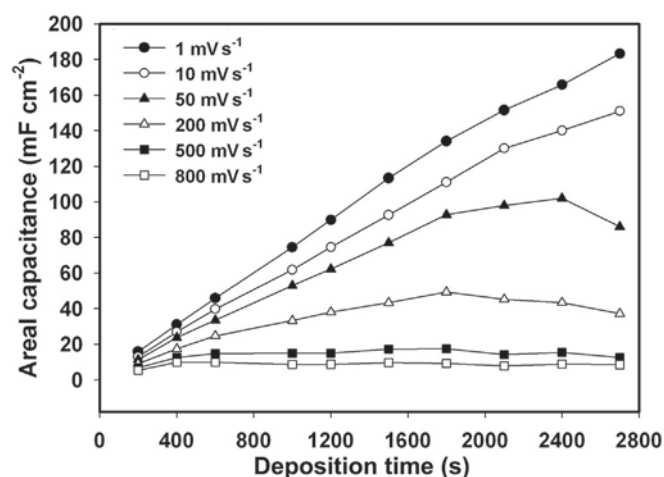


Fig. 4. Areal capacitance vs. deposition time plots for the PPy/GO electrodes with different CV scan rates.

The charge/discharge tests were also carried out at GCD current densities ranging from 0.1 to 2 mA cm^{-2} and the results are shown in Fig. 3b. During the process of charge/discharge, the electrochemical redox reaction between the electrode and electrolyte could be illustrated as: $\text{PPy}^+/\text{GO}^- + \text{K}^+ + \text{e}^- \leftrightarrow \text{PPy}^0/\text{GO}^-/\text{K}^+$. For a fully charged state of the cells, the anodic process was neutral because the PPy did not have any n-doping ability, the cathodic process was the fully oxidized state and charge neutrality was maintained by the GO^- ions. When the discharging process happened, the PPy in the cathodic process was reduced and the anode was oxidized to reach the same potential state, and the counter-ions ejected from the cathode were inserted in the anode electrode to maintain charge neutrality [42]. It is found from Fig. 3b that the charging curves are almost symmetric to their discharging counterparts in the whole potential region, and the similar triangular shapes demonstrate high power performance of the PPy/GO nanocomposites. As is shown in Fig. 3b, the areal capacitance of the PPy/GO nanocomposites reaches 22.8 mF cm^{-2} at 0.1 mA cm^{-2} , when the current density increases to 2 mA cm^{-2} , the areal capacitance reduced to 16 mF cm^{-2} , retaining $\sim 70\%$ of that at 0.1 mA cm^{-2} .

3.3. Effect of deposition time on the electrochemical behavior

Increasing the areal capacitance is significant for practical application of electrodes in supercapacitors, the previous investigations indicated adding the loading amount per unit area of

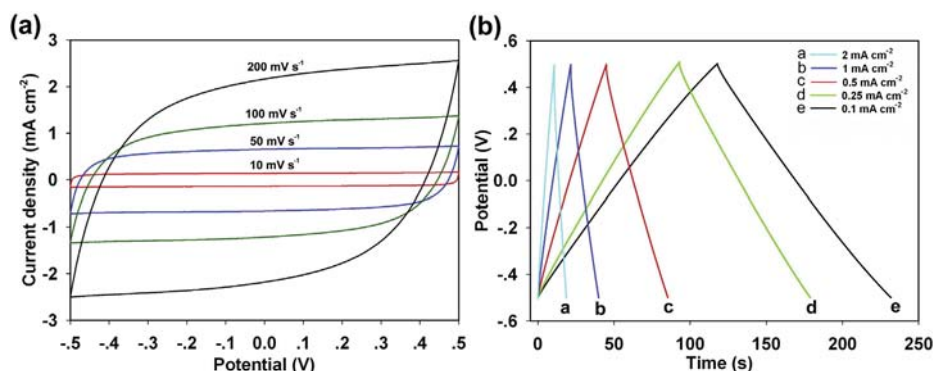


Fig. 3. (a) CV curves at different scan rates and (b) GCD curves at different GCD current densities of the capacitor cells assembled by 400 s-deposited PPy/GO electrodes.

active materials on the electrode could increase the areal capacitance [43]. Fortunately, the loading amount of the active materials on the electrodes made by electrochemical deposition can be easily adjusted by altering the deposition time. In this study, the effect of deposition time ranging from 200 s to 2700 s, namely, the loading amount of composites on the areal capacitance was investigated.

The areal capacitance versus deposition time plots for the PPy/GO nanocomposites electrodes with different CV scan rates are shown in Fig. 4. It can be observed that the areal capacitance nearly increase linearly as the adding of deposition time at the relatively low CV scan rates of 1 mV s^{-1} and 10 mV s^{-1} , and the dependence of the largest areal capacitance on varying scan rates and the corresponding deposition time is listed in Table 1. The highest areal capacitance of 152 mF cm^{-2} is obtained from the PPy/GO composites with the longest deposition time of 2700 s at the scan rate of 10 mV s^{-1} , far higher than that of PANI/graphite oxide composites (25 mF cm^{-2} at 5 mV s^{-1}) reported previously [18]. Furthermore, as the CV scan rate increases, the capacitance shows a general trend of decrease for the PPy/GO composites electrodes with every deposition time, which is due to the effective interaction between the matrix and the electrolyte will reduce greatly owing to the slow diffusion of ions in the matrix of polymer, in other word, only part of active materials on the electrode can be utilized in the process of fast CV scan. It is noteworthy that an interesting result can be observed from Fig. 4, that is except for the plots of 1 mV s^{-1} and 10 mV s^{-1} scan rates, the other plots do not show an upward trend all the time, the maximum capacitance value no longer appear at the longest deposition time of 2700 s. Moreover, Fig. 4 also shows that the incremental trend of areal capacitance value decrease gradually as the increase of scan rate, when the scan rate rise to 800 mV s^{-1} , the areal capacitance value is nearly independent with the deposition time excluding the few deposition time of 200 and 400 s. It can be attributed to the following reason, at the relatively low CV scan rate, the ions from the electrolyte have sufficient time to diffuse into the nanocomposites, so the active materials on the electrode can be used adequately, and then the more active materials would result in larger areal capacitance. However, as the increase of scan rate, the ions from electrolyte have no enough time to diffuse, which lead to part of active materials can be utilized, in addition, the thicker films would result in the larger diffusion resistance of electrolyte ions and increase electron transport resistance, so the longest deposition time of 2700 s-deposited electrode no longer exhibits the maximum areal capacitance value at relatively fast CV scans. When the scan rate became faster than 500 mV s^{-1} , the areal capacitance is no longer associated with the deposited amount of nanocomposites, which resulted from the only few active materials was used in the scan, so all the nanocomposites electrode of varying deposition time exhibit the nearly identical capacitance value.

In order to further investigate the impact of deposition time on electrochemical behavior, three types of electrodes including a short deposition time of 600 s, a moderate deposition time of

1800 s, and a long deposition time of 2700 s were compared detailedly. The SEM images of the three types of electrodes are shown in Fig. 5. A careful inspection of the structure of the PPy/GO nanocomposites suggests the electrodeposited PPy/GO nanocomposites are highly porous and consisted of two-dimensional composite nanosheets which interconnect with each other. GO sheets serve both as electroactive material and the scaffold for the deposition of the PPy, and all the three types of electrodes show the curly sheet-like morphology of the structure (see Fig. 5a, c, e). As expected, the cross section (see insets of Fig. 5a, c, e) SEM images display the thickness of as-prepared composites became thicker with the increment of deposition time and layered structure of the nanocomposites is observed. Meanwhile, a significant change can be observed from Fig. 5b, d and f is that the curly sheet become larger size with the increase of deposition time, and the 2700 s-deposited electrode display the maximum aggregation (see Fig. 5e). The results of SEM characterization suggest that the different deposition time has an obvious effect on the morphology of the PPy/GO nanocomposites, the longer deposition time would result in the morphology of larger size curly sheet.

The GCD tests were performed to characterize the capacitive performance of the three types of electrodes. Fig. 6a shows the charge/discharge curves of the three types of electrode at current density of 1 mA cm^{-2} , the results exhibit 2700 s-deposited electrode possesses the longest discharge time than the other two electrodes, its areal capacitance was 119.2 mF cm^{-2} , while 97 mF cm^{-2} for 1800 s-deposited electrode. However, when the current density increases to 5 mA cm^{-2} , the discharge time of 2700 s-deposited electrode is shorter than that of 1800 s-deposited electrode, but still longer than that of 600 s-deposited electrode, and then 1800 s-deposited electrode showed the areal capacitance of 70.2 mF cm^{-2} , which was larger than 56.2 mF cm^{-2} for 2700 s-deposited electrode. The results obtained from the GCD tests are consistent with those from the CV tests (see Fig. 4). Otherwise, an interesting result can be also observed from Fig. 6 is that the 1800 s-deposited electrode displays the lowest iR drop compared to the other two types of electrode at both 1 mA cm^{-2} and 5 mA cm^{-2} . The iR drop is usually caused by the overall internal resistance of the devices, and the low iR drop ought to be associated with the moderate amount of electroactive materials and the contact between the electroactive materials and electrode substrate. It should be pointed out that low internal resistance is of great importance in energy-storing devices as less energy will be wasted to produce unwanted heat during charging/discharging processes [44].

The aforementioned results manifest the longer deposited time would lead to larger areal capacitance at the relatively lower charge/discharge current density, which might be ascribed to two factors, one is due to the increase of electroactive materials on the electrode, the other is that PPy/GO nanocomposites exhibited more porous and large curly sheet-like morphology with the adding of deposition time according to the SEM characterization results, which could facilitate the diffusion of electrolyte into the active materials. Whereas, the more active materials deposited do not always reveal the larger capacitance, as the increase of charge/discharge current density, the thicker films would result in the larger diffusion resistance of electrolyte ions and increase electron transport resistance although it have more electroactive materials, so 1800 s-deposited electrode displayed larger capacitance than that of 2700 s-deposited electrode at larger current densities. It is noted that although 600 s-deposited electrode possesses the thinnest film, it remain shows the minimum areal capacitance value as it has few electroactive materials, so the moderate loading amount are more suitable for the fast charge/discharge.

As a steady state technique with small potential variation, EIS is more reliable for measuring the capacitance with minimized effect

Table 1
The dependence of the largest areal capacitance on varying CV scan rates and the corresponding deposition time.

Scan rate/ mV s^{-1}	The largest areal capacitance/ mF cm^{-2}	The corresponding deposition time/s
10	152	2700
30	117	2400
50	102	2400
100	77	1800
200	49	1800
500	18	1800

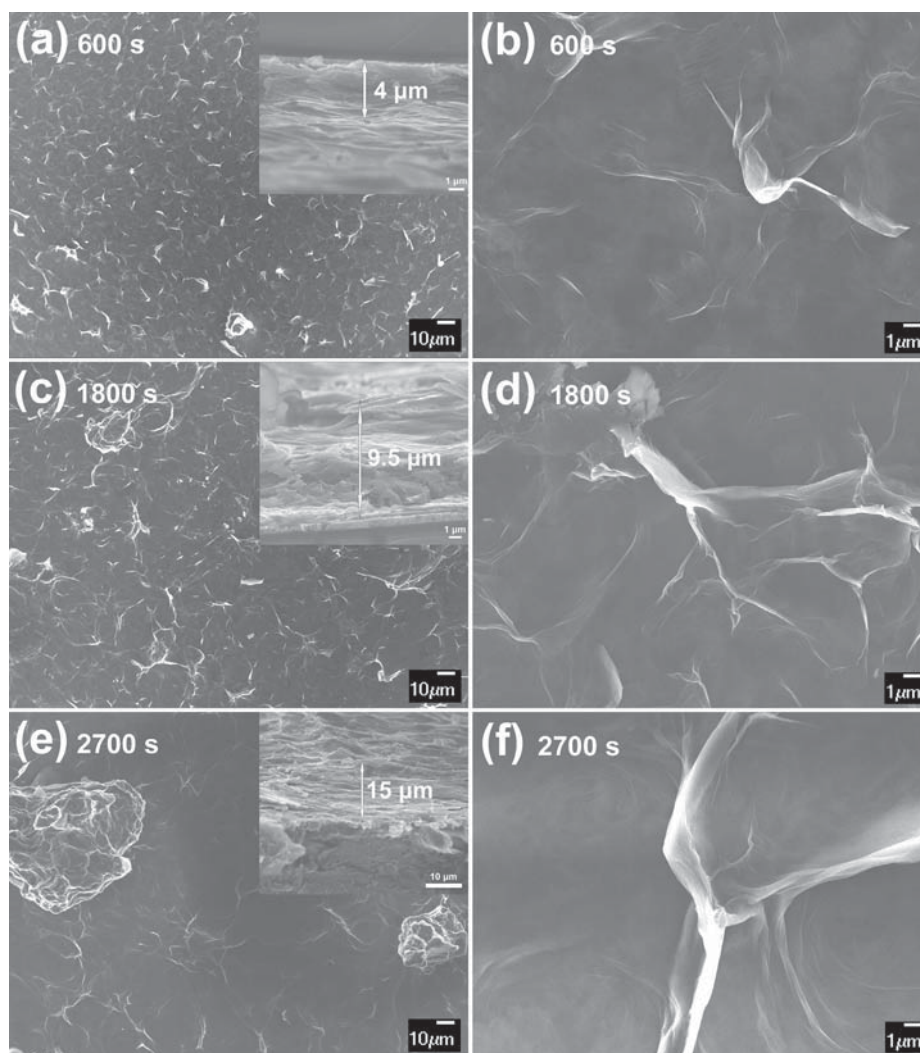


Fig. 5. The representative SEM images of the PPy/GO nanocomposites films obtained at (a,b) 600 s, (c, d) 1800 s, (e, f) 2700 s, and the insets show the cross-section SEM images of the corresponding composite films.

from non-capacitive Faradaic contributions and it can provide the electronic/ionic conductivity of the electrode materials during the charging/discharging progress [45]. Based on it, the three types of electrodes were studied by EIS and the resulting Nyquist plots at open-circuit potentials are illustrated in Fig. 7a, all the impedance plots are featured by a vertical trend at low frequencies, indicating

capacitive behavior according to the equivalent circuit theory. Furthermore, careful inspections of the plots at higher frequencies reveal a knee frequency, beyond which the capacitive behavior is replaced by the more inclined diffusion line, and the higher the knee frequency means the lower diffusion impedance and faster charge transfer rates [45]. The knee frequencies of the three types

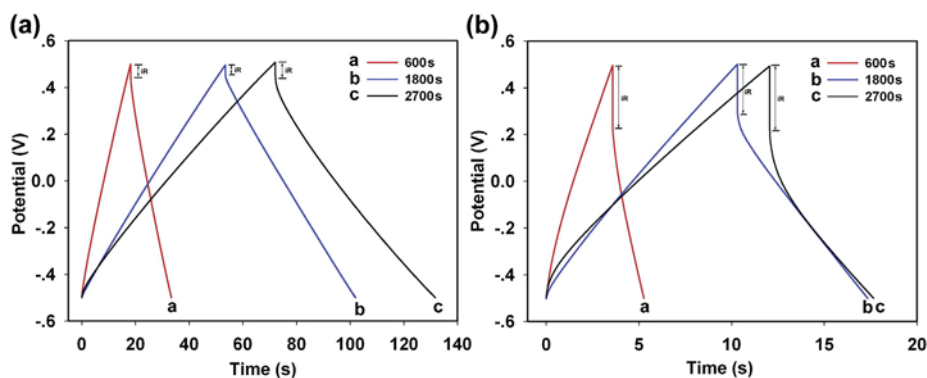


Fig. 6. GCD curves at the current densities of (a) 1 mA cm^{-2} and (b) 5 mA cm^{-2} for the capacitor cells assembled by 600 s, 1800 s, and 2700 s-deposited PPy/GO electrodes.

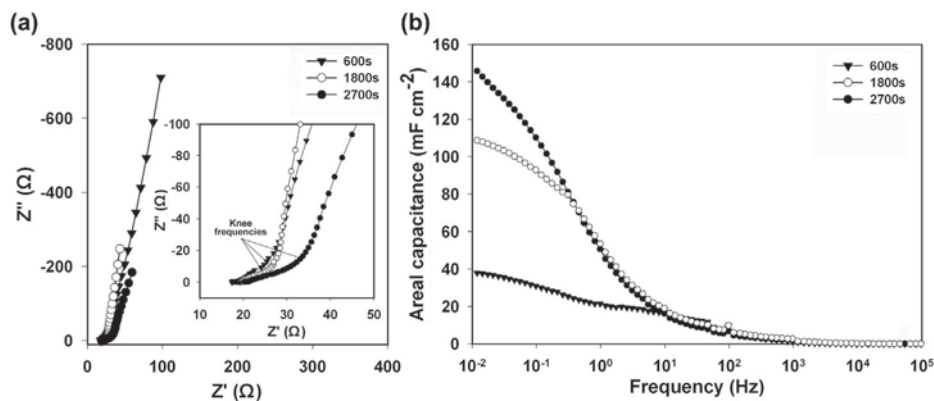


Fig. 7. (a) Nyquist plots of the capacitors assembled by 600 s, 1800 s, and 2700 s-deposited PPy/GO electrodes, insert is the EIS in high-frequency region and (b) the plots of areal capacitance vs. frequency for the PPy/GO electrodes.

of electrode are derived approximately from the enlarged Nyquist plots (the insets in Fig. 7a), knee frequencies of the three types of electrodes in numerical order are 600 s > 1800 s > 2700 s, successively, which indicate the thinner nanocomposites films possess much faster charge transfer rates as a result of the much lower diffusion resistance of ions from electrolyte. The results manifest too much electroactive materials would result in larger diffusion resistance of electrolyte ions and increase electron transport resistance with the increase of deposition amount, which are unfavorable for the rapid charge/discharge performance. The EIS results agree well with the CV and GCD tests results.

For electrochemical capacitors, the majority of their capacitance is only available at low frequency, so attention should be paid to the data in this range in the EIS spectra [46]. A straight line can be seen in the low frequency, the straight line of 1800 s-deposited electrode leans more towards imaginary axis, indicating that it has better capacitive character compared to 600 s and 2700 s-deposited electrodes. Fig. 7b presents the conversion capacitance obtained from EIS. The areal capacitance values of single electrode are obtained from the following Eq. (5) [47]:

$$C_S = -1/(\pi S f Z'') \quad (5)$$

Herein, C_S is the areal capacitance in $F\ cm^{-2}$, f is the frequency in Hz, Z'' the imaginary part of EIS in Ω , and S the geometric surface area of active materials on one electrode ($1\ cm^2$ in this research). With the frequency increases, the capacitance of all electrodes decreases, and at high-frequency region the capacitors behave like a pure resistance, which indicates that the electrolyte ions can not

be doped or undoped into the matrix at high frequencies. It is found that 1800 s-deposited electrode has a higher capacitance at high-frequency region and a lower capacitance at low-frequency region compared with those of 2700 s-deposited electrode, which is consistent with the data of CV and GCD tests. As expected, the capacitance values obtained from EIS are generally smaller than those CV values, but followed the same trend, which is mainly due to the different testing systems applied.

3.4. Ragone plot and cyclic stability

To illustrate the energy and power performance of the PPy/GO nanocomposites, a Ragone plot is shown in Fig. 8a. The 1800 s-deposited composites exhibits an energy density of $12.9\ \mu Wh\ cm^{-2}$ at a power density of $954.3\ \mu W\ cm^{-2}$, while it maintains $3.51\ \mu Wh\ cm^{-2}$ at $5763\ \mu W\ cm^{-2}$, which presents higher energy density and power density compared with previous reports on conducting polymers [18,48]. It should be noted that the energy density obviously decreases at high power density, some methods, such as appropriately change the deposited current density or adopting electrochemical deposition with template, may help to improve the rate capability of prepared electrode materials due to the preferable loose and porous microstructures.

The cycle life is a very important performance for the practical application, the stability of the cells assembled by the 1800 s-deposited PPy/GO composites electrode was evaluated using CV cycles at a scan rate of $100\ mV\ s^{-1}$ and the results are illustrated in Fig. 8b. The cycling measurements cause an increase in the

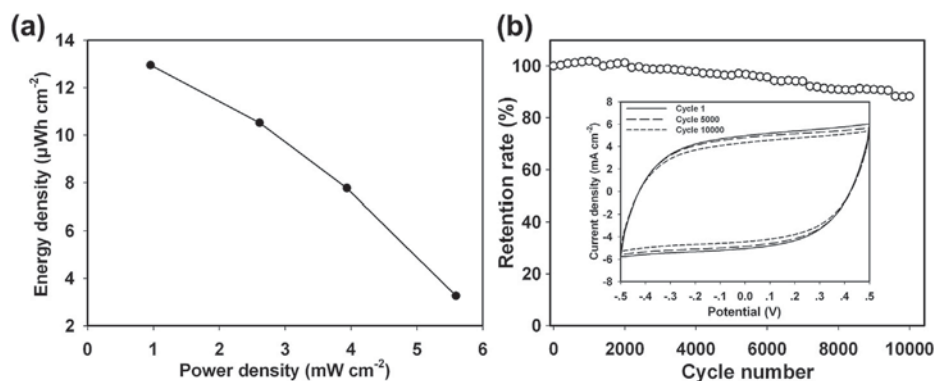


Fig. 8. (a) Ragone plot of 1800 s-deposited PPy/GO electrodes; (b) The relationship between capacitance retention ratio and cycling number for stability test at $100\ mV\ s^{-1}$ CV scan for 10,000 cycles.

capacitance up to 2000 cycles. It can be possibly related to a cycling measurement induced improvement in the surface wetting of the electrode, leading to more electroactive surface area [49,50]. The PPy/GO nanocomposites retain 96.4% of the initial capacitance after 5000 cycles, as well as persisting 88.3% for 10,000 cycles, highlighting the good electrochemical stability of the materials prepared. It is well known that conducting polymer-based electrodes usually suffers from a poor long-term stability during cycling because the swelling and shrinking of CPs may lead to degradation [51,52]. The improved stability for PPy/GO nanocomposites can be ascribed to the synergistic effect of GO and PPy and the layered structure of the nanocomposites, especially, the GO is dominant in the composites according the XPS and XRD tests (Fig. 2), resulting in the superior stability. Based on the discussion mentioned above, it is expected that the novel nanomaterials will be very promising for constructing electrochemical energy storage devices with improved performance.

4. Conclusions

In this study, we fabricated PPy/GO nanocomposites electrodes possessing large areal capacitance value using facile one-step electrochemical co-electrodeposition method, and what's more, this is the first time to report the areal capacitance of conducting polymer/graphene oxide nanocomposites as far as we are aware. The obtained PPy/GO composites exhibited superior electrochemical properties and cycling stability due to their synergistic effects. The loading amount of the composites could be easily tuned by changing the deposition time and the varying deposition time would have a noteworthy impact on their capacitive behavior. The longer deposited time would lead to larger areal capacitance at the relatively low charge/discharge current density, whereas, moderate loading amount are more suitable for the fast charge/discharge. In summary, the reported PPy/GO nanocomposites with large areal capacitance could be a qualified candidate for supercapacitor application. The electrochemical codeposition method presented here is very simple and effective, and it can be extended to fabricate flexible substrate based electrodes for future flexible electrochemical energy storage devices combining high power and high energy densities.

Acknowledgments

The authors appreciate funding from National Natural Science Foundation of China (21274082) and Shanxi Province (2012021021-3), the Program for New Century Excellent Talents in University (NCET-10-0926), and the Scientific Research Start-up Funds of Shanxi University (020351801002).

References

- [1] X.W. Yang, C. Cheng, Y.F. Wang, L. Qiu, D. Li, *Science* 341 (2013) 534–537.
- [2] G.P. Wang, L. Zhang, J.J. Zhang, *Chem. Soc. Rev.* 41 (2012) 797–828.
- [3] Z.S. Wu, Y. Sun, Y.Z. Tan, S.B. Yang, X.L. Feng, K. Mullen, *J. Am. Chem. Soc.* 134 (2012) 19532–19535.
- [4] K. Wang, Q.H. Meng, Y.J. Zhang, Z.X. Wei, M.H. Miao, *Adv. Mater.* 25 (2013) 1494–1498.
- [5] Z.J. Fan, J. Yan, T. Wei, L.J. Zhi, G.Q. Ning, T.Y. Li, F. Wei, *Adv. Funct. Mater.* 21 (2011) 2366–2375.
- [6] T. Zhai, F.X. Wang, M.H. Yu, S.L. Xie, C.L. Liang, C. Li, F.M. Xiao, R.H. Tang, Q.X. Wu, X.H. Lu, Y.X. Tong, *Nanoscale* 5 (2013) 6790–6796.
- [7] W. Chen, R.B. Rakhi, L.B. Hu, X. Xie, Y. Cui, H.N. Alshareef, *Nano. Lett.* 11 (2011) 5165–5172.
- [8] Z. Chen, J. Wen, C.Z. Yan, L. Rice, H. Sohn, M.Q. Shen, M. Cai, B. Dunn, Y.F. Lu, *Adv. Energy Mater.* 1 (2011) 551–556.
- [9] P. Simon, Y. Gogotsi, *Nat. Mater.* 7 (2008) 845–854.
- [10] G.D. Moon, J.B. Joo, Y.D. Yin, *Nanoscale* 5 (2013) 11577–11581.
- [11] Y.Z. Chang, G.Y. Han, J.P. Yuan, D.Y. Fu, F.F. Liu, S.D.A. Li, *J. Power Sources* 238 (2013) 492–500.
- [12] D.C. Zhang, X. Zhang, Y. Chen, P. Yu, C.H. Wang, Y.W. Ma, *J. Power Sources* 196 (2011) 5990–5996.
- [13] X. Wang, B.D. Myers, J. Yan, G. Shekhwat, V. Dravid, P.S. Lee, *Nanoscale* 5 (2013) 4119–4122.
- [14] W. Xing, C.C. Huang, S.P. Zhuo, X. Yuan, G.Q. Wang, D. Hulicova-Jurcakova, Z.F. Yan, G.Q. Lu, *Carbon* 47 (2009) 1715–1722.
- [15] H. Jiang, P.S. Lee, C.Z. Li, *Energy Environ. Sci.* 6 (2013) 41–53.
- [16] M.K. Liu, Y.E. Miao, C. Zhang, W.W. Tjiu, Z.B. Yang, H.S. Peng, T.X. Liu, *Nanoscale* 5 (2013) 7312–7320.
- [17] Z.C. Yang, C.H. Tang, Y. Zhang, H. Gong, X. Li, J. Wang, *Sci. Rep.-UK* 3 (2013).
- [18] H.G. Wei, J.H. Zhu, S.J. Wu, S.Y. Wei, Z.H. Guo, *Polymer* 54 (2013) 1820–1831.
- [19] C. Li, H. Bai, G.Q. Shi, *Chem. Soc. Rev.* 38 (2009) 2397–2409.
- [20] K. Zhang, L.L. Zhang, X.S. Zhao, J. Wu, *Chem. Mater.* 22 (2010) 1392–1401.
- [21] J.T. Zhang, P. Chen, B.H.L. Oh, M.B. Chan-Park, *Nanoscale* 5 (2013) 9860–9866.
- [22] Y.B. Tan, J.M. Lee, *J. Mater. Chem. A* 1 (2013) 14814–14843.
- [23] S. Biswas, L.T. Drzal, *Chem. Mater.* 22 (2010) 5667–5671.
- [24] P.A. Mini, A. Balakrishnan, S.V. Nair, K.R.V. Subramanian, *Chem. Commun.* 47 (2011) 5753–5755.
- [25] Y.S. Lim, Y.P. Tan, H.N. Lim, W.T. Tan, M.A. Mahnaz, Z.A. Talib, N.M. Huang, A. Kassim, M.A. Yarmo, *J. Appl. Polym. Sci.* 128 (2013) 224–229.
- [26] Y.S. Lim, Y.P. Tan, H.N. Lim, N.M. Huang, W.T. Tan, *J. Polym. Res.* 20 (2013) 156.
- [27] J.P. Liu, J. Jiang, M. Bosman, H.J. Fan, *J. Mater. Chem.* 22 (2012) 2419–2426.
- [28] Y.Y. Horng, Y.C. Lu, Y.K. Hsu, C.C. Chen, L.C. Chen, K.H. Chen, *J. Power Sources* 195 (2010) 4418–4422.
- [29] Y.Z. Chang, G.Y. Han, M.Y. Li, F. Gao, *Carbon* 49 (2011) 5158–5165.
- [30] Y.X. Xu, H. Bai, G.W. Lu, C. Li, G.Q. Shi, *J. Am. Chem. Soc.* 130 (2008) 5856–5857.
- [31] C.Z. Zhu, J.F. Zhai, D. Wen, S.J. Dong, *J. Mater. Chem.* 22 (2012) 6300–6306.
- [32] S. Konwer, R. Boruah, S.K. Dolui, *J. Electron. Mater.* 40 (2011) 2248–2255.
- [33] T.M. Wu, S.H. Lin, *J. Polym. Sci. Polym. Chem.* 44 (2006) 6449–6457.
- [34] R. Bissessur, P.K.Y. Liu, S.F. Scully, *Synth. Met.* 156 (2006) 1023–1027.
- [35] C. Bora, S.K. Dolui, *Polymer* 53 (2012) 923–932.
- [36] A. Osterholm, T. Lindfors, J. Kaupilla, P. Damlin, C. Kvarnstrom, *Electrochim. Acta* 83 (2012) 463–470.
- [37] Z. Weng, X.Y. Ni, *J. Appl. Polym. Sci.* 110 (2008) 109–116.
- [38] X.C. Li, G.L. Jiang, G.H. He, W.J. Zheng, Y. Tan, W. Xiao, *Chem. Eng. J.* 236 (2014) 480–489.
- [39] W. Fan, Y.Y. Xia, W.W. Tjiu, P.K. Pallathadka, C.B. He, T.X. Liu, *J. Power Sources* 243 (2013) 973–981.
- [40] H.L. Guo, X.F. Wang, Q.Y. Qian, F.B. Wang, X.H. Xia, *ACS Nano* 3 (2009) 2653–2659.
- [41] P. Manivel, S. Kanagaraj, A. Balamurugan, N. Ponpandian, D. Mangalaraj, C. Viswanathan, *Colloid. Surf. A* 441 (2014) 614–622.
- [42] G. Wallace, G. Spinks, *Soft Matter* 3 (2007) 665–671.
- [43] H. Fang, S.C. Zhang, X.M. Wu, W.B. Liu, B.H. Wen, Z.J. Du, T. Jiang, *J. Power Sources* 235 (2013) 95–104.
- [44] M. Jin, Y.Y. Liu, Y.L. Li, Y.Z. Chang, D.Y. Fu, H. Zhao, G.Y. Han, *J. Appl. Polym. Sci.* 122 (2011) 3415–3422.
- [45] C. Peng, J. Jin, G.Z. Chen, *Electrochim. Acta* 53 (2007) 525–537.
- [46] B.P. Bakhmatyuk, B.Y. Venhryn, I.I. Grygorchaka, M.M. Micov, *J. Power Sources* 180 (2008) 890–895.
- [47] K.S. Ryu, Y.G. Lee, K.M. Kim, Y.J. Park, Y.S. Hong, X.L. Wu, M.G. Kang, N.G. Park, R.Y. Song, J.M. Ko, *Synth. Met.* 153 (2005) 89–92.
- [48] K. Wang, W.J. Zou, B.G. Quan, A.F. Yu, H.P. Wu, P. Jiang, Z.X. Wei, *Adv. Energy Mater.* 1 (2011) 1068–1072.
- [49] Y.F. Xu, I. Hennig, D. Freyberg, A.J. Strudwick, M.G. Schwab, T. Weitz, K.C.P. Cha, *J. Power Sources* 248 (2014) 483–488.
- [50] H. Wang, C.M. Holt, Z. Li, X. Tan, B.S. Amirkhiz, Z. Xu, B.C. Olsen, T. Stephenson, D. Mitlin, *Nano Res.* 5 (2012) 605–617.
- [51] S. Sahoo, S. Dhibar, G. Hatui, P. Bhattacharya, C.K. Das, *Polymer* 54 (2013) 1033–1042.
- [52] H.L. Cao, X.F. Zhou, Y.M. Zhang, L. Chen, Z.P. Liu, *J. Power Sources* 243 (2013) 715–720.